JCI insight

Macrophage TGFβ signaling is critical for wound healing with heterotopic ossification after trauma

Nicole K. Patel, … , Amanda K. Huber, Benjamin Levi

JCI Insight. 2022. https://doi.org/10.1172/jci.insight.144925.

Research In-Press Preview **Bone biology** **Immunology**

Transforming growth factor beta 1 (TGFβ1) plays a central role in normal and aberrant wound healing, but the precise mechanism in the local environment remains elusive. Here, using a mouse model of aberrant wound healing resulting in heterotopic ossification (HO) after traumatic injury, we find autocrine TGFβ1 signaling in macrophages, and not mesenchymal stem/progenitor cells (MPCs), is critical in HO formation. In-depth single cell transcriptomic and epigenomic analyses in combination with immunostaining of cells from the injury site demonstrate increased TGFβ1 signaling in early infiltrating macrophages, with open chromatin regions in TGFβ1 stimulated genes at binding sites specific for transcription factors of activated TGFβ1 (SMAD2/3). Genetic deletion of TGFβ1 receptor type 1, (*Tgfbr1*;*Alk5*) in macrophages, results in increased HO, with a trend toward decreased tendinous HO. To bypass the effect seen by altering the receptor we administered a systemic treatment with TGFβ1/3 ligand trap TGFβRII-Fc, which results in decreased HO formation and a delay macrophage infiltration to the injury site. Overall, our data support the role of the TGFβ1/ALK5 signaling pathway in HO.

Macrophage TGFβ Signaling is Critical for Wound Healing with Heterotopic Ossification after Trauma

Nicole K. Patel, MD[1]*, Johanna H. Nunez, MD[3]*, Michael Sorkin, MD[1], Simone Marini, PhD[2], Chase A. Pagani, BA[1,3], Amy L. Strong, MD[1], Charles D. Hwang, MD[1], Shuli Li, PhD[1], Karthik R. Padmanabhan PhD[4], Ravi Kumar, PhD[5], Alec C. Bancroft, BSA[3], Joey A. Greenstein[1], Reagan Nelson[1], Husain A. Rasheed[1], Nicholas Livingston[3], Kaetlin Vasquez, MS[1], Amanda K. Huber, PhD[1]*, Benjamin Levi, MD[1,3]*†

Section of Plastic Surgery, Department of Surgery, The University of Michigan Medical School, Ann Arbor, MI, USA[1]; Department of Epidemiology and Emerging pathogens institute, University of Florida, Gainesville, FL, USA[2]; Department of Surgery, UT Southwestern Medical Center, Dallas, TX, USA[3]; Epigenomics Core, The University of Michigan Medical School, Ann Arbor, MI, USA[4]; Acceleron Pharma, Inc., Cambridge, MA, USA[5]; Both authors contributed equally*

Change in Current Affiliations: CH is currently in Division of Plastic and Reconstructive Surgery, Harvard medical school, Massachusetts General Hospital, Boston, MA, USA. MS is currently an Assistant Professor Plastic and Reconstructive Surgery at Ohio State University Columbus OH. KRP is currently a Staff Scientist at Takara Bio San Francisco, CA. RK is currently Chief Science Officer of Acceleron, A whole-owned subsidiary of Merck & Co., Inc.

Cambridge, MA, USA. AKH Department of Radiation Oncology, Cancer Biology, The University of Michigan Medical School, Ann Arbor, MI, USA

Key Words: Transforming growth factor beta, heterotopic ossification, macrophages, mesenchymal stem cells, ligand trap

†Corresponding author: Benjamin Levi, MD. Lee-Hudson Profession and Division Chief of General Surgery. Associate Professor in Plastic and Reconstructive Surgery and General Surgery, UT Southwestern Medical Center, 5323 Harry Hines Blvd., Building E, 5th floor, Room 514A, Dallas, TX 75390-9158; Tel: 214-633-7680; Email: Benjamin.Levi@UTSouthwestern.edu

Conflicts of Interest:

TGFβRII-Fc was provided by Acceleron and they performed and provided results for SPR analysis and Cell based assays. Several authors (NKP, RK, BL, MS) are named on a patent for TGFβRII-Fc use in traumatic HO.

Disclosure:

NKP, MS, CH, SL, RK, BL are on an abstract submitted to plastic surgery research conference (2018) for which a small portion of the preliminary data was part of an abstract.

Abstract:

Transforming growth factor beta 1 (TGFβ1) plays a central role in normal and aberrant wound healing, but the precise mechanism in the local environment remains elusive. Here, using a mouse model of aberrant wound healing resulting in heterotopic ossification (HO) after traumatic injury, we find autocrine TGFβ1 signaling in macrophages, and not mesenchymal stem/progenitor cells (MPCs), is critical in HO formation. In-depth single cell transcriptomic and epigenomic analyses in combination with immunostaining of cells from the injury site demonstrate increased TGFβ1 signaling in early infiltrating macrophages, with open chromatin regions in TGFβ1 stimulated genes at binding sites specific for transcription factors of activated TGFβ1 (SMAD2/3). Genetic deletion of TGFβ1 receptor type 1, (*Tgfbr1*;*Alk5*) in macrophages, results in increased HO, with a trend toward decreased tendinous HO. To bypass the effect seen by altering the receptor we administered a systemic treatment with TGFβ1/3 ligand trap TGFβRII-Fc, which results in decreased HO formation and a delay macrophage infiltration to the injury site. Overall, our data support the role of the TGFβ1/ALK5 signaling pathway in HO.

Introduction:

Transforming growth factor beta (TGFβ) signaling is essential for normal tissue-specific regeneration and aberrant wound healing. The response to injury following a traumatic event can be divided into hemostasis, inflammation, proliferation, maturation and remodeling (1). In each stage of healing, TGFβ plays a number of critical roles that vary in context and in a cell type-dependent manner, including regulation of cell proliferation, differentiation, migration, invasion, and chemotaxis of fibrotic and immune cells (2, 3). Specifically, in normal fracture healing, TGFβ plays a pivotal role by enhancing the proliferation and differentiation of mesenchymal stem/progenitor cells (MPCs), increasing the production of extracellular matrix, and acts as a chemoattractant to osteoblasts (4). TGFβ has also been shown to play a key role in cartilage formation and increases the formation of callus and bone strength (5). In vivo experiments have demonstrated accelerated fracture healing and enhanced bone remodeling with TGFβ (6, 7). Similarly, aberrant ectopic bone formation or heterotopic ossification (HO) following trauma injury or hip arthroplasty has been shown to have increased TGFβ expression near the injury or surgical site (8-10). Overexpression of TGFβ in tendon has been shown to induce spontaneous HO, whereas TGFβ neutralizing antibody attenuates ectopic bone formation in traumatic mouse models (9). These findings support the critical role of TGFβ in both normal and abnormal wound healing in the bone, but the precise mechanism by which TGFβ acts on the surrounding local environment and myeloid cells remains to be fully elucidated.

Both infiltrating immune cells, specifically monocytes and macrophages, and MPCs participate in the process of both normal and aberrant bone formation after injury or trauma (10, 11). Specifically, TGFβ1 produced by macrophages has been shown to stimulate chondrogenesis in MPCs (10, 12), which is a fundamental process for endochondral ossification. In addition to

chondrogenesis, TGFβ1 signaling in macrophages has been shown to modify immunogenicity through altering cell polarization and migration, which has been shown to further promote bone formation (13-15). Activation by TGFβ1 results in heterodimerization of TGFβRII with TGFβRI, also known as activin receptor-like kinase 5 (ALK5) and allows for downstream canonical TGFβ signaling, which involves phosphorylation of SMAD2/3 and translocation of pSMAD2/3 to the nucleus to activate gene transcription (16). *Alk5* deletion in monocytes has been shown to inhibit pro-inflammatory and promote anti-inflammatory macrophage markers of expression (17). Gong et al. demonstrated that while knocking out TGFβRII in hematopoietic cells did not affect the efferocytotic ability of macrophages, it resulted in the inability of macrophages to upregulate M2-polarized genes (18). Our group and others have shown that TGFβ1 expression, specifically by myeloid cells, is critical to HO formation after traumatic injury (9, 10). In the mouse model for traumatic HO, deletion of macrophage *Tgfb1* resulted in decreased HO formation. Furthermore, treatment with a CD47 activating peptide decreased macrophage TGFβ1 expression, skewed macrophage polarization away from an M2 phenotype towards a more resident macrophage phenotype and resulted in decreased HO (10). However, it is unknown whether the TGFβ1 produced by macrophages further alters the macrophage phenotype and function or impacts the local wound environment to alter matrix production or differentiation of MPCs (19, 20).

In the current study, we investigated the impact of TGFβ signaling in macrophages and the MPCs in the local wound environment. Utilizing a mouse model of HO and single cell transcriptomic and epigenomic analyses, we found specific increases in TGFβ stimulated gene expression as well as open chromatin regions at pSMAD2/3 binding sites in TGFβ1 stimulated genes in macrophages and MPCs. Overall, the findings are suggestive of an autocrine effect of

TGFβ1 in macrophages. Targeted deletion of *Alk5* in macrophages (*LysMCre*) further corroborated the autocrine effect of TGFβ receptor signaling on macrophages, which was not observed with deletion of *Alk5* in MPCs (*Hoxa11CreER*^{T2}). Due to some additional effects seen in macrophage receptor deletion, we opted to treat upstream of the receptor by targeting the TGFβ ligands. Treating injured mice systemically with a ligand trap, TGFβRII-Fc, which blocks both TGFβ1 and TGFβ3 ligand, resulted in attenuated HO formation and in delayed macrophage infiltration. Taken together, these findings suggest that macrophage ALK5 signaling potentiates aberrant bone formation and that pharmacological inhibition of TGFβ1 with the ligand trap TGFβRII-Fc, is a potential therapeutic agent to prevent HO.

Results:

Increased canonical TGFβ signaling at the HO site after burn and tenotomy

Increased TGFβ activity has been shown to be present in human HO tissue (9). When TGFβ1 binds to its receptor, SMAD2/3 is phosphorylated and translocates to the nucleus, which then activates target genes responsible for a variety of cell specific functions (21-39). We therefore examined the canonical signaling pathway in mice by assessing percent area of phosphorylated SMAD3 (pSMAD3) in HO anlagen at 1 week and 3 weeks post injury. Similar to what has been previously described, we found a trend toward greater pSMAD3 staining from the HO injury site after 1 week, 3.7 ± 0.9%, and at 3 weeks, 3.3± 0.9%, compared to uninjured hind limb 2.3 ± 0.2% (Figure 1, Supplemental Figure 1). Both MPCs and macrophages express the receptor for and can respond to TGFβ1, therefore, we analyzed TGFβ1 signaling by pSMAD3 specifically in these populations. MPCs, marked by PDGFRα, had increased percent of cells pSMAD3 positive at 3 weeks (89.7 ± 3.8%) compared to 1 week (75.5 ± 6.3%, p=0.0819) (Figure 2A-C, Supplemental Figure 2). Alternatively, percent of the infiltrating tissue macrophages that were pSMAD3 positive at 1 week and 3 weeks post injury were similar and very high at 97.4 ± 0.2% and 96.9 ± 3.1% respectively (p=0.8657)(Figure 2D-F, Supplemental Figure 3A-C). Increased pSMAD3 in MPCs and the near ubiquitous signaling in macrophages following injury suggests TGFβ signaling is present or upregulated in these cell populations in our trauma induced HO model early on, before the process of cartilage formation has started.

Changes in TGFβ stimulated genes in trauma induced HO

Our group and others have shown TGFβ1, specifically expressed by myeloid cells, is critical to HO formation after traumatic injury (9, 10). While we see increased TGFβ signaling at

the HO anlagen, it is unknown whether TGFβ1 expressed by macrophages during a traumatic injury acts in an autocrine or paracrine fashion, and in which cell type this signaling is necessary for the formation of HO. To begin to assess this, we used single cell RNA sequencing (scRNA-seq) performed on cells harvested from the hindlimbs at days 0 (uninjured), 7, and 21 post-burn/tenotomy (GSE126060). Workflow for scRNA-seq is shown in Figure 3A. Clustering was done as previously characterized. MPC clusters were identified based on their expression of *Pdgfrα* and *Prrx1* (Figure 3B-C)(40). Macrophage (Mac) clusters were identified based on high expression of known markers *Lyz2* and *Cd14* (Figure 3B-C). The MPC and Mac clusters were assessed for genes known to be transcribed upon TGFβ stimulation. When we looked at these TGFβ stimulated genes in the Macs, we found 15 genes known to be controlled through TGFβ signaling, many important in the immune function of macrophages, increased at day 7 compared to uninjured including; *Apoe, Cebpb, Fn1, Il1b, Cxcr4, Mmp14, Plaur, Bhlhe40, Tgm2, Itgav, Timp1, Arg1, Olr1, Ell2, and Trem1* (Figure 3D). Analysis of MPC specific TGFβ stimulated genes revealed 15 genes highly increased at day 7. These genes were important in the production of, attachment to, or reorganization of the extracellular matrix including: *Fn1, Col1a1, Col1a2, Col3a1, Col5a2, Timp1, Mmp14, Mmp2, Lox, Angptl4, Tpm1, Marcksl1, Acta2, Ltbp2, and Kif26b* (Figure 3E). Because increases in TGFβ isoforms and their receptors might suggest increased TGFβ specific signaling, we also analyzed the gene expression of these elements in our scRNA-seq data (Figure 4A). In the MPCs, none of the genes for TGFβ or their receptors are appreciably changed in expression levels across time (Figure 4A). Conversely, in the macrophages there is increased expression of *Tgfb1*, *Tgfbr1*, and *Tgfbr2* at day 7*,* with no change in other TGFβ isoforms (2 or 3), or *Tgfbr3* (Figure 4A). In fact, the macrophages demonstrated equal or greater TGFβ and receptor expression levels than the MPCs.

To get a better understanding of the genomic regulation of these TGFβ stimulated genes in the Mac and MPC clusters, in a separate data set we performed single nucleus ATAC sequencing (scATAC-seq) on cells from the HO site of day 0 (uninjured) and 7 after injury. We evaluated the accessibility of chromatin around the known DNA binding sequence for pSMAD2/3 in the genes for the TGFβ ligands and receptors. In the macrophages, there was openness in promoter regions near SMAD2/3 binding sites for *Tgfb1*, *Tgfbr1*, *Tgfbr*2, corresponding to our scRNA-seq findings (Figure 4B). The MPCs showed some increased openness in these genes at SMAD2/3 binding sites; however, the change was more prominent in the macrophages. (Figure 4B). Next, we analyzed chromatin accessibility at SMAD2/3 binding sites in the 15 Mac and 15 MPC TGFβ1 stimulated genes at day 7, identified above. In MPCs 12/15 genes and in the Macs 8/15 genes had open chromatin in SMAD2/3 binding sites in TGFβ1 stimulated genes identified (Supplemental Figure 4). Altogether this data confirms the histological data that canonical TGFβ signaling is occurring in both macrophages and MPCs at the HO anlagen after injury with greater change in TGFβ ligand and receptor levels in macrophages.

Early HO site macrophages display TGFβ ligand-receptor pairs

Based on our previous data, macrophage infiltration into to the HO site is at its peak 3 days after injury (10), therefore, we assessed cells at day 0 and day 3 post-injury from the HO anlagen and performed scRNA-seq (GSE126060). After sequencing, we identified 16 distinct clusters corresponding to known cell types and we isolated the 3 clusters with macrophage cell type into cluster 1, based on same expression markers mentioned above (Figure 5A-B). These

composite macrophage clusters were used for subsequent analysis in addition to the canonical analysis with day 7.

To get a better understanding of the putative autocrine TGFβ signaling that might be occurring in these early infiltrating macrophages, we performed receptor-ligand pairing analysis. To do this, a list of all potential ligands and receptors was adapted from human to mice (41) and was compared against cellular features present in our scRNA-seq data sets, of which 1044 are applicable. The top 100 ligand receptor pairs expressed in the macrophages at our HO site on day 3 or 7 was subsequently used. This list was cross-referenced to confirm the expression of the ligands' cognate receptors within the same macrophages. This resulted in a list of 100 receptor-ligand pairs. Of these pairs, pathways associated with growth factor signaling, like TGFβ1, was identified (Figure 5C). The data suggests early macrophage autocrine TGFβ signaling after traumatic injury plays a role in HO formation.

TGFβRI/ALK5 perturbation in MPCs and macrophages.

We next set out to determine whether ALK5 signaling in macrophages, MPCs or both is important to HO formation after traumatic injury. To do this, we used a mouse with either myeloid or MPC specific deletion of *Alk5*. To do this we targeted the TGFβ1 receptor type 1, TGFβRI; encoded by *Alk5*, using $Alk5^{fl/fl}$ mice. To delete *Alk5* in MPCs we chose to cross our $Alk5^{fl/fl}$ mice with the $Hoxa11CreER^{T2}$ mouse line creating $Hoxa11CreER^{T2}; Alk5^{fl/fl}$ mice (42). Hoxa11 is a homeobox transcription factor expressed specifically in the zeugopod (radius/ulna, tibia/fibula). Although *Hox* genes are important in patterning during embryonic development (43), *Hoxa11* has been shown to mark mesenchymal stem/progenitor cells throughout life (42). Work in our laboratory has demonstrated that these Hoxa11 expressing cells are those that form

HO in our model (44). These mice allowed conditional deletion of *Alk5* only in the zeugopod region by administration of tamoxifen prior to inducing injury, thus avoiding adverse effect of *Alk5* deletion during development. MicroCT analysis 9 weeks after injury in the *Hoxa11CreER^{T2}; Alk5$^{fl/fl}$* mice revealed no statistical difference in the amount of HO formed (Figure 6A-B).

Next, we evaluated the role of ALK5 signaling in macrophages, by crossing with the *LysMCre* mouse line (*LysMCre;Alk5$^{fl/fl}$)*. We found, that *LysMCre+/-;Alk5$^{fl/fl}$* mice developed increased volume of HO compared to *LysMCre-/-;Alk5$^{fl/fl}$* littermate controls (6.07 ± 1.03 mm^3 3.81 ± 0.34 mm^3 (p=0.02, N=7 and 2 respectively). In our tentotomy model of HO, ectopic bone forms at 2 distinct anatomic sites: 1) growing off of the calcaneaus (bone associated HO) and 2) growing off of the proximal cut end of the tendon (tendinous HO; Supplemental Figure 5A) Specifically, we found, that *LysMCre+/-;Alk5$^{fl/fl}$* mice developed increased bone associated/distal HO compared to littermate controls (Figure 6C-D). In contrast, we found that there was not an increase in tendinous HO and there was actually a decrease in this region (though not statistically significant; Figure 6D). We therefore, wondered whether this difference was due to the different macrophage populations in tendon and bone. Bone associated resident macrophages, those marked by CD169 (45), might be important drivers of HO, whereas tendinous HO might be driven by circulating macrophages. We confirmed by histology that CD169$^+$ macrophages, not thought to be marked by the *LysmCre* allele, were ALK5$^+$ across multiple timepoints (day 0, 3, 7, and 21) in both the endosteum and periosteum (Supplemental Figure 5B). Therefore, we set out to block this TGFB/TGFBR signaling cascade through upstream blockade of the TGFβ1 and β3 ligands which should effect both macrophage populations.

TGFβRII-Fc treatment decreased early cavernous bone and mature bone in vivo

We used a ligand trap (TGFβRII-Fc) to determine if the bone associated bone effect observed could be circumvented. Before use in vivo, we first tested the equilibrium binding constant of the TGFβRII-Fc using surface plasmon resonance. Our results show TGFβ1 and β3 have a K_D of 14.8 pM and 11.2 pM respectively compared to K_D of 11600 pM for TGFβ2 (Table. 1). Subsequently, the IC_{50} was determined using an A549 luciferase reporter cell line for TGFβ signaling, including TGFβ1, TGFβ2 and TGFβ3. After the addition of the TGFβRII-Fc, the IC_{50} was calculated to be 22.9 pM and 4.46 pM for TGFβ1 and β3 respectively but greater than 88000 for TGFβ2 (Table. 1). Overall, this data indicated the ligand trap had much greater affinity for binding TGFβ1 and β3 with little effect on TGFβ2.

Next, to evaluate the TGFβRII-Fc treatment on trauma induced HO formation, we used our mouse model for trauma induced HO. After injury, mice were administered either vehicle or TGFβRII-Fc (10mg/kg; twice weekly) by subcutaneous injection for 3 weeks. We chose to treat these mice for the 3 weeks based on our previous paper using inhibitors of BMP signaling receptors, similar *Alk* gene family members, in our model of HO (46). Further, we chose subcutaneous injection as previous studies of antibody injection using this route of administration show that the antibody is taken up into the systemic circulation (47). HO sites were harvested at both 3 weeks for histology and 9 weeks for microCT analysis (Figure 7A). Safranin O staining, for glycosaminoglycans and cartilage formation, demonstrated decreased early cavernous bone formation in mice treated with TGFβRII-Fc compared to vehicle (Figure 7B). Next, we analyzed mature bone at 9 weeks post injury by uCT and found there was decreased bone formation by 3D reconstruction in the TGFβRII-Fc treatment animals, specifically proximal bone volume (0.03 ± 0.02 mm^3 compared to vehicle 1.45 ± 0.51 mm^3,

p=0.026 (Figure 7C)). HO trabecular volume and porosity were significantly decreased in the TGFβRII-Fc treated group (4.68 ± 2.33 mm^3 to 1.28 ± 0.63 mm^3, p=0.016 and 0.45 ± 0.05 mm^3 to 0.024 ± 0.04 mm^3, p=0.013, respectively (Supplemental Figure 6A-B)). Importantly, we found that there was no difference in tibial cortical thickness in TGFβRII-Fc treated mice (Supplemental Figure 6C). Treatment with TGFβRII-Fc decreased bone formed away from the tendon injury site, and to a lesser degree in the region of injury.

TGFβRII-Fc treatment does not overtly affect MPC canonical TGFβ1 signaling or proliferation

Studies have shown that macrophages lacking TGFβ receptor on their surface inhibits both migration and M2 polarization (18). Therefore, we sought to determine if the effects of TGFβRII-Fc treatment on TGFβ canonical signaling are indeed on the macrophages and not the TGFβ signaling of the MPCs at the HO site by histology. In support of this, we found no appreciable difference by IF in MPC TGFβ signaling (signified by percent of PDGFRα$^+$ cells that are nuclear pSMAD3$^+$) in the TGFβRII-Fc treated group compared to vehicle treated controls (46.5 ± 4.7% vs 46.8 ± 5.6%, p=0.9671 (Figure 8A-B)). Further, quantification of the cell count by quantification of number of nuclei in the injury site demonstrated that there was a trend toward overall decreased cells in the TGFβRII-Fc treated group (160.7 ± 20.5 vs 125.0 ± 9.1 cells, p=0.1628) as well as a decrease in cell count of PDGFRα$^+$ cells (82.3 ± 12.3 vs 59.8 ± 6.9 cells, p=0.1607), and a decrease in the percent of total cells that are PDGFRα$^+$ (52.2 ± 4.7% vs 47.5 ± 2.9%, p=0.4169 (Figure 8C-E)). Analysis of proliferation by Ki-67 staining revealed the percent of MPCs (PDGFRα$^+$ cells) that were Ki-67$^+$ was not different with TGFβRII-Fc treatment compared to control (12.9 ± 4.8% vs. 13.3 ± 2.1%, p=0.9385 (Figure 8F-G)). Together,

there are no appreciable changes in MPC TGFβ signaling or proliferation when treated with the ligand trap.

TGFβRII-Fc modulates injury site inflammation

TGFβ ligands are also known to be important drivers of immune cell recruitment during inflammation. TGFβ has been shown to stimulate chemotaxis of neutrophils and macrophages (15, 48-52); therefore, we sought to determine if TGFβRII-Fc treatment affected immune cell infiltration, particularly macrophages, into the HO site. Immunofluorescent imaging of the HO site for the macrophage marker F4/80 in TGFβRII-Fc treated or vehicle control mice 1-week post injury demonstrated that mice treated with TGFβRII-Fc had a decrease in the percent of F4/80+ cells (17.9 ± 5.5% vs. 7.2 ± 3.7%, p=0.2000 (Figure 8H-I)) at the HO anlagen. This suggests that TGFβRII-Fc treatment acts by altering macrophage migration to the site of injury. Further, flow cytometry of cells from the extremity injury in the treatment group and vehicle control for days 5, 7 and 14 (Figure 9A), show decreased myeloid cells, CD45+CD11b+, and percentage across time points, independent of treatment group (Figure 9B, F). The change in myeloid cells after injury echoes previous reports (10). There is no significant change between the treatment groups in the percentage of neutrophils at each time point (Figure 9C, G). However, there is a decrease in neutrophil total cell count numbers, a trend also seen with monocytes and macrophages across time points (Figure 9D-E, H-I). The percent of monocytes in the tissue at day 14, show a significant decrease when treated with the ligand trap (15.7% vs 8.3%, p=0.03), with a trend toward decreased monocyte numbers earlier with treatment (Figure 9E, H). In the treatment condition, total macrophage count is significantly decreased at day 7 (4734448 vs 205884 cell

count, p=0.03)) (Figure 9I). In summary, this data demonstrates that TGFβRII-Fc modulates HO formation and macrophage migration.

Discussion:

Traumatic heterotopic ossification is a debilitating and complex pathological process where endochondral ossification occurs secondary to injury and inflammation. Mesenchymal stem/progenitor cells are known to undergo aberrant differentiation in the development and progression of HO. Inflammatory cells, specifically myeloid cells, have also recently been shown to play a central role in this form of aberrant wound healing (9, 10). Prior studies have demonstrated that targeting macrophage TGFβ expression can hamper the formation of HO (10). However, it is unknown whether TGFβ signaling via ALK5 exerts its effects in the macrophages through an autocrine loop, or on MPC differentiation via a paracrine role.

There is extensive literature on TGFβ ligands participating in wound healing, particularly in aberrant wound healing such as fibrosis and ectopic bone formation (10, 53-57). TGFβ1 is a master regulator after acute injury (53), interacting with almost every cell type involved. TGFβ1 has been shown to lead to fibroblast migration (3) and activation (58) into an injury site. Elevated levels of TGFβ1 at a wound site results in recruitment of circulating inflammatory cells such as neutrophils and macrophages (53). Macrophages, in turn, migrate to the wound site and secrete cytokines including more TGFβ1. Macrophages with an anti-inflammatory, immune-suppressive, pro-angiogenic and pro-regenerative phenotype, classified as M2, are known to produce TGFβ1; TGFβ1 signaling in the macrophage itself has been suggested to play an important role in polarization to this “alternate” phenotype (18). Here we show there is increased TGFβ downstream signaling in MPCs and macrophages at the HO site; changes in expression of

TGFβ ligands and receptors; and changes in chromatin accessibility. With the addition of ligand-receptor pair analysis in early infiltrating macrophages, we suggest that TGFβ is playing an autocrine role.

Selective genetic deletion of ALK5 in *LysmCre*$^{+}$ myeloid cells increased bone associated HO. The increased HO pattern in this genetic model is inconsistent with the results of systemic TGFβRII-Fc administration where there is a decrease in proximal HO, located at the retracted proximal tendon stub status post tenotomy. The same proximal pattern is seen in our prior study in which TGFβ1 was altered in macrophages genetically or with CD47 activating peptide (10). Unlike the proximal HO pattern, the distal pattern did not present in our previous study. It is possible, the HO increase in *LysmCre;Alk5*$^{fl/fl}$ mice could be a result of CD169^{+} bone macrophages, distinct from osteoclasts. Bone macrophages are known to impact osteoblast differentiation and bone mineralization (59). The macrophages might not express *LysMCre* and thus retain the receptor, and ultimately have unmitigated TGFβ signaling (45). Alternatively, the TGFβ receptor complex is heterodimeric receptor consisting of 2 types (TGFβR1 and TGFβR2) and there is evidence that loss of TGFβR1 (ALK5) could have ongoing signaling through TGFβR2. Such that loss of both receptor types is necessary to completely stop TGFβ signaling (60, 61). Another possibility is that the loss of *Alk5* in macrophages also alters their migration and polarization so profoundly they are unable to become a more regenerative macrophage, which has some salubrious effects to limit the bone associated HO. Future studies using more flow and newer modalities such as spatial transcriptomics, might be able to provide clarity on if there are population differences spatially in the regions of HO anlagen. We decided to focus less on the pathophysiology of this unintended effect, but on finding a way to altogether bypass the

receptor signaling by altering signaling at the ligand level, which is why we utilized a ligand trap (TGFβRII-Fc) with the added benefit of being a more feasible treatment option.

With the ligand trap (TGFβRII-Fc) treatment, we noted decreased proximal/tendinous HO. Our IF and flow cytometry data looking at the HO anlagen site 1 week after injury demonstrates there are decreased monocyte/macrophages at the site with ligand treatment suggesting a delay in monocyte/macrophage migration to the injury site. Though not statistically significant, a similar decreasing trend of HO was seen in the *LysmCre;Alk5*$^{fl/fl}$ mice. Previous research has shown inhibition of ALK5 alone can impair monocyte migration toward TGFβ1(52). Our findings support that the trend toward decreased tendinous HO noted in the *LysmCre;Alk5*$^{fl/fl}$ mice is also due to impaired monocyte/macrophage migration.

It is well documented in the literature that TGFβ1 is an important factor in chondrogenesis (62), cartilage, and joint formation (63). In fact, the effects of TGFβ's on MPCs has been shown to be complex and context dependent. Latent and soluble forms of TGFβ through alternative pathways can drive human mesenchymal stem cells to chondrogenesis (64). Studies have shown that the latent form signals through an integrin mediated pathway (65). Whilst others have shown there are mechanotransducive effects, such as the ROCK pathway, that augment the signaling of TGFβ (66). Additionally, hypoxia plays a role in signaling (67).

Given how the literature is so demonstrative toward TGFβ's pro-chondrogenic effects, it begs the question of why in our study the loss of TGFβRI signaling specifically in MPCs, resulted in no significant change in HO formation after traumatic injury. Data presented by Wang et al. where TGFβRI functions in cartilage to block BMP signaling in resting growth plate chondrocytes does support our findings (60). Therefore, in our MPC specific deletion mice, chondrocytes formed from MPCs would not have BMP signaling inhibited by TGFβRI signaling,

and this drives the formation of HO. Additionally, it has been shown that deletion of both TGFβRI and TGFβRII is necessary for complete signaling inhibition in TGFβ1 signaling (61, 68).

Currently, effective management of HO is limited, with prophylactic NSAIDs or radiation therapy offering only modest benefit (69). Surgical excision can be done but has substantial chance of recurrence. For example, in elbow HO there is around 20% recurrence following surgical excision (70). To expand and improve treatment options, we need to understand the underlying signaling pathways to find potential targets for therapy. Mouse models have shown a non-selective TGFβ neutralizing antibody attenuates HO formation in a tendon puncture model (9). A primate HO model suggests aberrant bone is mediated by TGFβ1 and in human HO tissue there are elevated levels of TGFβ, suggesting the role of TGFβ ligands on HO formation is conserved across species (9, 71). Therefore, therapeutic targeting of TGFβ ligands has the potential to mitigate the burden of HO.

We demonstrate that macrophages are the critical target of TGFβRI signaling for aberrant wound healing after traumatic injury. We also show that systemic treatment with TGFβRII-Fc modulates TGFβ signaling upstream of the TGFβRI, impairing monocyte/macrophage migration, such that HO formation is attenuated, particularly in the proximal region. This data signifies that targeting TGFβ ligands and macrophage autocrine signaling after traumatic injury is an effective future therapeutic target to improve wound healing and prevent aberrancies such as muscle fibrosis (54) or HO.

Methods:

Mouse Use and Treatments:

Mice were housed in standard conditions. All animals used were C57BL/6 background mice. C57BL/6 mice were purchased from The Jackson Laboratory (000664). All mice received pre-operative and 48 hours post-operative SQ buprenorphine (0.06mg/kg) for analgesia. Animals were anesthetized with inhaled isoflurane. Mice received 30% total body surface area partial-thickness dorsal burn. The dorsal burn was induced using a metal block heated to 60°C in a water bath and applied to the dorsum for 18 seconds continuously. Tenotomy was performed by transection of the left Achilles tendon. Animals were either assigned to the vehicle control or ligand trap group. Vehicle control was 1X PBS and ligand trap was muTGFbRII-mFc, shortened to TGFβRII-Fc, supplied by Acceleron Pharma, Inc. Treatment began day of surgery (day 0). Mice were administered vehicle or ligand trap (10mg/kg) subcutaneously twice weekly for 3 weeks. Mice were euthanized for experiments at 1, 3, or 9 weeks post injury for experimental analysis.

Hoxa11CreER^{T2} and *LysMCre* were bred in house with *Alk5 $^{fl/fl}$*. The *Hoxa11CreER^{T2}* line was obtained from Dr. Deneen Wellik at the University of Wisconsin, Madison. These were then crossed with the Alk5$^{fl/fl}$ line that was obtained from Dr. Katherine Gallagher at the University of Michigan to produce *Hoxa11CreER^{T2};Alk5$^{fl/fl}$* mice. To induce the deletion of *Alk5, Hoxa11CreER^{T2};Alk5$^{fl/fl}$* mice were placed on Tamoxifen chow for 3 weeks when they were 5 weeks of age. *LysMCre* mice were crossed with *Alk5$^{fl/fl}$* mice, both from the Jackson Laboratory, to generate *LysMCre;Alk5$^{fl/fl}$*. Littermates of both crosses were used as controls. Mice underwent the burn/tenotomy injury described above. Legs were harvested at 9 weeks and MicroCT analysis was performed. *CD169Cre* mice were obtained from Riken Group (RBRC06239) (72, 73). *CD169Cre* mice were crossed with *Rosa26-tdTomato* to obtain double heterozygous mice. They underwent our injury model and tissue harvested for immunofluorescent histology.

Single cell RNA sequencing (scRNA-seq) analysis:

Single cell data replicates from day 0 (uninjured), 3, 7 and 21 post-injury were taken from GSE126060 (10). We considered cells and genes as per our previous analysis (44). Briefly, we selected replicates to have a consistent number of cells for each time point: day 0 (replicates 1-4, 3815 cells), day 3 (replicates 1-2, 4201 cells), day 7 (replicate 1, 3405 cells), and day 21 (replicates 1-3, 3505 cells) for multi time-point analyses (43). Cells were retained based on genes expressed in more than 10 cells (17131 genes), total expressed genes in the range of [500, 5000], and the fraction of mitochondrial gene UMIs lower than 0.2. Counts were normalized (default parameters) and scaled (regressing against number of genes expressed per cell and fraction of mitochondrial expression). Variable genes were extracted (default Seurat parameters) and defined as the intersection of the top 5000 genes for each replicate (1497 genes). Replicates were joined via canonical correlation analysis (20 components, using the overall variable genes). Sixteen cell populations (numbered 0 to 15) were obtained with Louvain algorithm, resolution 0.4, using the aligned canonical correlation components. FindMarkers (default Seurat parameters) was utilized to extract the markers from each population. Markers were ranked according to the difference in the fractions of cells expressing each marker within the population versus rest of the considered cells. Top markers were used to label the cell populations.

Multi time-points analyses:

Two analyses were set-up in Seurat 3.1.4 (73), considering 3 time points (0, 7, and 21); and 2 time points (0 and 3). Each analysis consisted of subsetting genes, cell counts, and cell identities (clusters) from the joined set described above. For each analysis, the subset data were

merged. After merging, data was processed by normalization, identification of variable genes, scaling, dimensional reduction (PCA), and non-linear dimensional reduction (UMAP). The first fifteen dimensions were used for the UMAP projection, while default parameters were kept for all the other steps. The 16 cell populations from prior analysis (44) were then merged and labeled as ten final clusters according to their identity. More specifically, we merged multiple macrophages clusters (1, 2, 4), mesenchymal clusters (0, 6, 8), endothelial clusters (2, 5), and pericyte/smooth muscle clusters (9, 11). The MPC cluster as well as the Mac cluster were used for subsequent analysis. Individual genes were assessed in MPC or Mac clusters for expression levels across time points. Gene expression markers for MPC cluster or Mac cluster were generated in comparison to rest of cells/clusters for each time point. Gene expression markers for MPC cluster or Mac cluster were generated in comparison to rest of cells/clusters for each time point based on prior analysis by our group (43). Individual genes were assessed in MPC or macrophage clusters for expression levels across time points.

Macrophage Ligand-Receptor pair analysis:

To perform receptor ligand pairing analysis on our Mac cluster, a list of all potential ligands was adapted from a human ligand receptor database (44) for mice. There were a total of 1372 unique mouse genes for ligands and receptors. Of these, 1044 were expressed in our Mac cluster. We considered days 3 and 7 independently. Ligand and receptor genes were ranked according to the average counts per cell in the Mac cluster. The ligand-receptor pairs including to the top 100 ranked ligands and receptors were used to create circle plots.

Single cell ATAC sequencing (scATAC-seq) analysis and genome tracks:

Single cell ATAC sequencing was performed using Signac 3.1.5 (https://github.com/timoast/signac) as previously described by our group using GSE150995 (44). Data from day 0 and day 7 were combined after filtering the dataset to cells that have at least 100 features. The combined Seurat object was then normalized using the default set of parameters, and top variable peak accessibilities were calculated using a cutoff of at least 20 cells. Dimension reduction was done using t-SNE with dimensions 2 through 30 used as input features. A shared nearest neighbor modularity optimization-based algorithm with a resolution of 0.2 was used to determine unique clusters. Clusters from scRNA-seq data were used to guide the labeling of clusters using the FindTransferAnchors function. The MPC cluster of cells was isolated and bigwig files were generated for each day using sinto (https://timoast.github.io/sinto/) and deeptools (74). BigWig files were uploaded into the open source software, integrated genomics viewer (75, 76). The data range for the open chromatin tracks (day 0 and 7, Mac cluster, and 2 MPC clusters) was set from 0 to 800 across all tracks. The SMAD binding element was input to evaluate motif (77). Genes were assessed for open chromatin in promoter regions.

Surface Plasmon Resonance (SPR) analysis:

All analyses were performed with a Biacore T100 instrument (GE Healthcare). An anti-mouse Fc-specific antibody was immobilized on a Series S CM5 sensor chip through amine coupling by following the manufacturer's instructions (GE Healthcare). HBS-EP buffer (GE Healthcare) supplemented with 350 mM NaCl and 0.5 mg/ml bovine serum albumin (BSA) was used as running buffer. TGFβRII-Fc was captured on the experimental flow cell at a density of ~50 RUs. TGFβ1 and TGFβ3 (0.013 nM – 10 nM) and TGFβ2 (0.04 nM - 90 nM) were injected in three-fold serial dilution over the captured protein for 300 seconds, followed by 600 seconds

dissociation time at a flow rate of 70 µL/min with buffer blanks injected periodically for double referencing. The chip regeneration was performed with 10 mM glycine pH 1.7. All sensorgrams were processed by double referencing (subtraction of the responses from the reference surface and from an average of blank buffer injections). To obtain kinetic rate constants, TGFβ1 and TGFβ3 data were fit to 1:1 interaction model which includes a term for mass transport using BIAevaluation software (GE Healthcare). A concentration range of 0.013 nM -1.1 nM for both TGFβ1 and TGFβ3 was used to fit TGFβRII-Fc binding sensorgrams. The equilibrium binding constant K_D was determined by the ratio of binding rate constants k_d/k_a. Due to the transient nature of binding, the equilibrium binding constant K_D of TGFβ2 was determined by using the steady-state affinity model, where the maximal measured signal (in RU) before the end of the association phase (which is close to be a plateau) is plotted against the ligand concentration, which ranges from 0.12 nM to 90 nM for TGFβ2 binding.

Cell-based assays:

The cell-based assay utilizes A549 cells (human lung carcinoma cell line, CCL-185, ATCC). A549 cells were seeded in 48-well plates at $6.5x10^4$ cells per well in F-12K medium (ATCC) supplemented with 10% FBS and incubated overnight. All incubations were at 37ºC, 5% CO_2 unless otherwise noted. The cells were transiently co-transfected with both the luciferase vector pGL3 $(CAGA)_{12}$ in which the firefly luciferase gene expression is under the control of the TGF-β ligand responsive $(CAGA)_{12}$ element, and the constitutively active renilla luciferase plasmid pRL-CMV to normalize for transfection efficiency. This was done by combining 10 µg pGL3$(CAGA)_{12}$, 0.1 µg pRL-CMV, and 30 µL XtremeGENE9 (Roche) with 970 µL Opti-MEM (Thermo Fisher) and incubating the mixture for 30 minutes at room

temperature prior to adding 24 mL of assay buffer (F-12K supplemented with 0.1% BSA) and applying to the plated cells (500 µL/well) for an overnight incubation. The next day, 3-fold serial dilutions of TGFβRII-Fc were made in assay buffer in a separate 48-well plate (eight data points starting at 100 ng/mL (TGFβ1 assay), 25,000 ng/mL (TGFβ2 assay) or 75 or 100 ng/mL (TGFβ3 assay)). The final concentration of TGFβ1, TGFβ2 or TGFβ3 added to the corresponding wells in this plate was 640 pg/mL, 480 pg/mL and 270 pg/mL, respectively. The receptor/ligand mixture was incubated for 30 min prior to applying 500 µL/well to the transfected A549 cells. The cells were harvested after an 18-20h incubation and assayed using the Dual Luciferase Reporter Assay system (Promega, with a Tecan Infinite M200 instrument) to determine normalized luciferase activity expressed as RLU (relative luciferase units).

Histology:

Legs were decalcified, embedded and sectioned as previously described by our lab (78). Safranin O staining was done on tissue cross-sections from 3 weeks post-burn/tenotomy. Brightfield images of cross-sections were obtained (n=2).

Immunofluorescence:

Immunofluorescence was done as previously described (10). Briefly, sections were washed in 1X TBS with 0.05% Tween-20 (TBST), incubated in donkey block at room temperature for 1-2 hours, and then primary antibodies in antibody diluent were applied and incubated at 4ºC overnight. Primary antibodies were washed off with TBST. Slides were incubated with donkey secondaries for 1 hour at room temperature. Subsequently, slides were washed with TBST, counterstained with Hoechst and mounted with prolong glass (Invitrogen,

P36980). Details regarding antibodies and stains can be found in Table 2. Immunofluorescent images were obtained with Leica SP8 confocal inverted microscope or Leica STELLARIS 8.

Microscopy image quantification:

Image area quantifications were performed in FIJI (79). The pSMAD3 percent area was obtained first by converting 20x images of the pSMAD3 channel to 8-bit. Intermodules threshold was applied to encompass positive signal. Results were measured and exported to excel. All cell counts were performed by hand within the LASX software on either 20x or 63x zoomed in images and exported to excel for subsequent calculations.

Micro Computerized Topography (MicroCT):

Left legs were scanned using Bruker SkyScan 1176 MicroCT. Bone volumes were determined utilizing microCT imaging (35 uM resolution, 357 uA beam energy, 70 kV beam current, 520 ms exposure). Scans were analyzed using calibrated imaging protocol as previously described by MicroView micro CT viewer (GE Health Care and Parallax Innovations) (80). Bone reconstructions depicting representative means of treatment groups were calculated at 800 HU. Ectopic bone was manually splined and measured at 0, 800, and 1250 Hounsfield Unit (HU) thresholds. Ectopic bone volumes were characterized as total volume, proximal, distal, bone associated, and tendinous.

Flow Cytometry:

Following a burn tenotomy injury, at timepoints of 5, 7, and 14 days, the soft tissue from the posterior compartment between the muscular origin and the calcaneal insertion of the

Achilles tendon was dissected out and collected for processing. The tissue was digested for 20-30 min in 0.3% Type 1 Collagenase and 0.4% Dispase II (Gibco) in Roswell Park Memorial Institute (RPMI) medium at 37 °C under constant agitation at 180 rpm. The digestions were quenched with 10% FBS in RPMI and then filtered through 40μm sterile strainers. Specimens were blocked with anti-mouse CD16/32 and subsequently stained using the antibodies Ly6G, CD11b, Ly6C, and/or CD45 as described in Table 2. Samples were washed with FACs buffer (2%FBS in PBS) and then flow cytometry data was collected using a FACSCanto (BD). Analysis was performed using FlowJo software.

Statistics:

For microscopy quantifications, statistical analyses were performed in Prism 8 where associated graphs were also generated. Sharpiro-Wilk was applied to assess for normality. Students T-test was used for parametric data and data are represented by mean ± SEM. Mann-Whitney U-Test was performed on non-parametric data and median ± quartile. For microCT, statistical analyses were performed in IBM SPSS Statistics 24 and Prism 8. Graphs were created in Prism GraphPad 7 or Excel. Shapiro-Wilk Test was used to determine the appropriate test. Two-way independent t-tests were performed on parametric data at $\alpha=0.05$, p-value significance indicated by *. Mann-Whitney U-Test was performed on non-parametric data at $a=0.05$, p-value significance indicated by $^{\#}$. One-way ANOVA with Brown-Forsythe test for correction as well as Dunnett's multiple comparison was performed on data at $\alpha=0.05$.

Study Approval:

All animal experiments described were approved by the University Committee on the Use and Care of Animals at the University of Michigan, Ann Arbor (PRO0007930) and University of Texas Southwestern, Dallas (2020-102949). All animal procedures were carried out in accordance with the guidelines provided in the *Guide for the Use and Care of Laboratory Animals: Eighth Edition* from the Institute for Laboratory Animal Research (81).

Acknowledgements:

We would like to thank the University of Michigan Center for Molecular Imaging and the Biomedical Research Core Facilities Microscopy Imaging Core for their assistance. We would like to thank Noelle Visser and Nicole J. Edwards for technical assistance. MS funded by Plastic Surgery Foundation National Endowment Award. CH supported by Howard Hughes Medical Institute Medical Research Fellowship. BL funded by NIH 1R01AR079863, NIHR01AR079171. AKH funded by the IFOPA ACT grant, CaBRI Research Grant for Rare Diseases.

Author Contributions:

Nicole K. Patel: Conception and design, collection and/or assembly of data, data analysis and interpretation, manuscript writing

Johanna H. Nunez: Conception and design, collection and/or assembly of data, data analysis and interpretation

Michael Sorkin: Conception and design, collection and/or assembly of data, data analysis and interpretation

Simone Marini: Single cell data analysis and interpretation, manuscript reading and editing

Chase A. Pagani: Data analysis and interpretation, manuscript writing

Amy L. Strong: Data analysis and interpretation, manuscript writing

Charles Hwang: Data analysis and interpretation

Shuli Li: Conception and design

Karthik R. Padmanaban: single cell ATAC sequencing analysis and pathway analysis

Ravi Kumar: Conception and final approval of manuscript

Alec C. Bancroft: Data analysis and interpretation

Joey A. Greenstein: Data analysis and interpretation

Reagan Nelson: Data analysis and interpretation

Husain Rasheed: Data analysis and interpretation

Nicholas Livingston: Data analysis and interpretation

Kaetlin Vasquez: Data analysis and design

Amanda K. Huber: Conception and design, data analysis and interpretation, collection and/or assembly of data, manuscript editing and final approval of manuscript.

Benjamin Levi: Conception and design, data analysis, final approval of manuscript

References:

1. Gurtner GC, Werner S, Barrandon Y, and Longaker MT. Wound repair and regeneration. *Nature.* 2008;453(7193):314-21.
2. Morikawa M, Derynck R, and Miyazono K. TGF-β and the TGF-β Family: Context-Dependent Roles in Cell and Tissue Physiology. *Cold Spring Harb Perspect Biol.* 2016;8(5).
3. Lichtman MK, Otero-Vinas M, and Falanga V. Transforming growth factor beta (TGF-β) isoforms in wound healing and fibrosis. *Wound Repair Regen.* 2016;24(2):215-22.
4. Dimitriou R, Tsiridis E, and Giannoudis PV. Current concepts of molecular aspects of bone healing. *Injury.* 2005;36(12):1392-404.
5. Barnes GL, Kostenuik PJ, Gerstenfeld LC, and Einhorn TA. Growth factor regulation of fracture repair. *J Bone Miner Res.* 1999;14(11):1805-15.
6. Wildemann B, Schmidmaier G, Ordel S, Stange R, Haas NP, and Raschke M. Cell proliferation and differentiation during fracture healing are influenced by locally applied IGF-I and TGF-beta1: comparison of two proliferation markers, PCNA and BrdU. *J Biomed Mater Res B Appl Biomater.* 2003;65(1):150-6.
7. Ozkan K, Eralp L, Kocaoglu M, Ahishali B, Bilgic B, Mutlu Z, et al. The effect of transforming growth factor beta1 (TGF-beta1) on the regenerate bone in distraction osteogenesis. *Growth Factors.* 2007;25(2):101-7.
8. Suutre S, Toom A, Arend A, and Selstam G. Bone tissue content of TGF-beta2 changes with time in human heterotopic ossification after total hip arthroplasty. *Growth Factors.* 2009;27(2):114-20.
9. Wang X, Li F, Xie L, Crane J, Zhen G, Mishina Y, et al. Inhibition of overactive TGF-β attenuates progression of heterotopic ossification in mice. *Nat Commun.* 2018;9(1):551.
10. Sorkin M, Huber AK, Hwang C, Carson WF, Menon R, Li J, et al. Regulation of heterotopic ossification by monocytes in a mouse model of aberrant wound healing. *Nat Commun.* 2020;11(1):722.
11. Convente MR, Wang H, Pignolo RJ, Kaplan FS, and Shore EM. The immunological contribution to heterotopic ossification disorders. *Curr Osteoporos Rep.* 2015;13(2):116-24.
12. Matsunobu T, Torigoe K, Ishikawa M, de Vega S, Kulkarni AB, Iwamoto Y, et al. Critical roles of the TGF-beta type I receptor ALK5 in perichondrial formation and function, cartilage integrity, and osteoblast differentiation during growth plate development. *Dev Biol.* 2009;332(2):325-38.
13. Shull MM, Ormsby I, Kier AB, Pawlowski S, Diebold RJ, Yin M, et al. Targeted disruption of the mouse transforming growth factor-beta 1 gene results in multifocal inflammatory disease. *Nature.* 1992;359(6397):693-9.
14. Beck LS, Ammann AJ, Aufdemorte TB, Deguzman L, Xu Y, Lee WP, et al. In vivo induction of bone by recombinant human transforming growth factor beta 1. *J Bone Miner Res.* 1991;6(9):961-8.
15. Wahl SM, Hunt DA, Wakefield LM, McCartney-Francis N, Wahl LM, Roberts AB, et al. Transforming growth factor type beta induces monocyte chemotaxis and growth factor production. *Proc Natl Acad Sci U S A.* 1987;84(16):5788-92.

16. Ebner R, Chen RH, Shum L, Lawler S, Zioncheck TF, Lee A, et al. Cloning of a type I TGF-beta receptor and its effect on TGF-beta binding to the type II receptor. *Science.* 1993;260(5112):1344-8.
17. Li W, Wang J, and Li Z. ALK5 deficiency inhibits macrophage inflammation and lipid loading by targeting KLF4. *Biosci Rep.* 2020;40(3).
18. Gong D, Shi W, Yi SJ, Chen H, Groffen J, and Heisterkamp N. TGFβ signaling plays a critical role in promoting alternative macrophage activation. *BMC Immunol.* 2012;13:31.
19. Watt FM, and Huck WT. Role of the extracellular matrix in regulating stem cell fate. *Nat Rev Mol Cell Biol.* 2013;14(8):467-73.
20. Meng XM, Nikolic-Paterson DJ, and Lan HY. TGF-beta: the master regulator of fibrosis. *Nat Rev Nephrol.* 2016;12(6):325-38.
21. Furumatsu T, Tsuda M, Taniguchi N, Tajima Y, and Asahara H. Smad3 induces chondrogenesis through the activation of SOX9 via CREB-binding protein/p300 recruitment. *J Biol Chem.* 2005;280(9):8343-50.
22. Gratchev A, Kzhyshkowska J, Kannookadan S, Ochsenreiter M, Popova A, Yu X, et al. Activation of a TGF-beta-specific multistep gene expression program in mature macrophages requires glucocorticoid-mediated surface expression of TGF-beta receptor II. *J Immunol.* 2008;180(10):6553-65.
23. Ashcroft GS. Bidirectional regulation of macrophage function by TGF-beta. *Microbes Infect.* 1999;1(15):1275-82.
24. Wahl SM, McCartney-Francis N, Allen JB, Dougherty EB, and Dougherty SF. Macrophage production of TGF-beta and regulation by TGF-beta. *Ann N Y Acad Sci.* 1990;593:188-96.
25. Hall MC, Young DA, Waters JG, Rowan AD, Chantry A, Edwards DR, et al. The comparative role of activator protein 1 and Smad factors in the regulation of Timp-1 and MMP-1 gene expression by transforming growth factor-beta 1. *J Biol Chem.* 2003;278(12):10304-13.
26. Falcone DJ, McCaffrey TA, Mathew J, McAdam K, and Borth W. THP-1 macrophage membrane-bound plasmin activity is up-regulated by transforming growth factor-beta 1 via increased expression of urokinase and the urokinase receptor. *J Cell Physiol.* 1995;164(2):334-43.
27. Sanjabi S, Oh SA, and Li MO. Regulation of the Immune Response by TGF-beta: From Conception to Autoimmunity and Infection. *Cold Spring Harb Perspect Biol.* 2017;9(6).
28. Ramji DP, Singh NN, Foka P, Irvine SA, and Arnaoutakis K. Transforming growth factor-beta-regulated expression of genes in macrophages implicated in the control of cholesterol homoeostasis. *Biochem Soc Trans.* 2006;34(Pt 6):1141-4.
29. Wahl SM, Allen JB, Weeks BS, Wong HL, and Klotman PE. Transforming growth factor beta enhances integrin expression and type IV collagenase secretion in human monocytes. *Proc Natl Acad Sci U S A.* 1993;90(10):4577-81.
30. Xu Y, Tabe Y, Jin L, Watt J, McQueen T, Ohsaka A, et al. TGF-beta receptor kinase inhibitor LY2109761 reverses the anti-apoptotic effects of TGF-beta1 in myelo-monocytic leukaemic cells co-cultured with stromal cells. *Br J Haematol.* 2008;142(2):192-201.
31. Boutard V, Havouis R, Fouqueray B, Philippe C, Moulinoux JP, and Baud L. Transforming growth factor-beta stimulates arginase activity in macrophages.

Implications for the regulation of macrophage cytotoxicity. *J Immunol.* 1995;155(4):2077-84.
32. Abnaof K, Mallela N, Walenda G, Meurer SK, Sere K, Lin Q, et al. TGF-beta stimulation in human and murine cells reveals commonly affected biological processes and pathways at transcription level. *BMC Syst Biol.* 2014;8:55.
33. Renzoni EA, Abraham DJ, Howat S, Shi-Wen X, Sestini P, Bou-Gharios G, et al. Gene expression profiling reveals novel TGFbeta targets in adult lung fibroblasts. *Respir Res.* 2004;5:24.
34. Verrecchia F, Chu ML, and Mauviel A. Identification of novel TGF-beta /Smad gene targets in dermal fibroblasts using a combined cDNA microarray/promoter transactivation approach. *J Biol Chem.* 2001;276(20):17058-62.
35. Zhao W, Wang C, Liu R, Wei C, Duan J, Liu K, et al. Effect of TGF-beta1 on the Migration and Recruitment of Mesenchymal Stem Cells after Vascular Balloon Injury: Involvement of Matrix Metalloproteinase-14. *Sci Rep.* 2016;6:21176.
36. Kim ES, Kim MS, and Moon A. TGF-beta-induced upregulation of MMP-2 and MMP-9 depends on p38 MAPK, but not ERK signaling in MCF10A human breast epithelial cells. *Int J Oncol.* 2004;25(5):1375-82.
37. Kurpinski K, Lam H, Chu J, Wang A, Kim A, Tsay E, et al. Transforming growth factor-beta and notch signaling mediate stem cell differentiation into smooth muscle cells. *Stem Cells.* 2010;28(4):734-42.
38. Popova AP, Bozyk PD, Goldsmith AM, Linn MJ, Lei J, Bentley JK, et al. Autocrine production of TGF-beta1 promotes myofibroblastic differentiation of neonatal lung mesenchymal stem cells. *Am J Physiol Lung Cell Mol Physiol.* 2010;298(6):L735-43.
39. Xie J, Wang C, Huang DY, Zhang Y, Xu J, Kolesnikov SS, et al. TGF-beta1 induces the different expressions of lysyl oxidases and matrix metalloproteinases in anterior cruciate ligament and medial collateral ligament fibroblasts after mechanical injury. *J Biomech.* 2013;46(5):890-8.
40. Hwang C, Marini S, Huber AK, Stepien DM, Sorkin M, Loder S, et al. Mesenchymal VEGFA induces aberrant differentiation in heterotopic ossification. *Bone Res.* 2019;7:36.
41. Ramilowski JA, Goldberg T, Harshbarger J, Kloppmann E, Kloppman E, Lizio M, et al. A draft network of ligand-receptor-mediated multicellular signalling in human. *Nat Commun.* 2015;6:7866.
42. Pineault KM, Song JY, Kozloff KM, Lucas D, and Wellik DM. Hox11 expressing regional skeletal stem cells are progenitors for osteoblasts, chondrocytes and adipocytes throughout life. *Nat Commun.* 2019;10(1):3168.
43. Wellik DM, and Capecchi MR. Hox10 and Hox11 genes are required to globally pattern the mammalian skeleton. *Science.* 2003;301(5631):363-7.
44. Huber AK, Patel N, Pagani CA, Marini S, Padmanabhan K, Matera DL, et al. Immobilization after injury alters extracellular matrix and stem cell fate. *J Clin Invest.* 2020.
45. Batoon L, Millard SM, Wullschleger ME, Preda C, Wu AC, Kaur S, et al. CD169(+) macrophages are critical for osteoblast maintenance and promote intramembranous and endochondral ossification during bone repair. *Biomaterials.* 2019;196:51-66.
46. Agarwal S, Loder SJ, Breuler C, Li J, Cholok D, Brownley C, et al. Strategic Targeting of Multiple BMP Receptors Prevents Trauma-Induced Heterotopic Ossification. *Mol Ther.* 2017;25(8):1974-87.

47. Sumbria RK, Zhou QH, Hui EK, Lu JZ, Boado RJ, and Pardridge WM. Pharmacokinetics and brain uptake of an IgG-TNF decoy receptor fusion protein following intravenous, intraperitoneal, and subcutaneous administration in mice. *Mol Pharm.* 2013;10(4):1425-31.
48. Fava RA, Olsen NJ, Postlethwaite AE, Broadley KN, Davidson JM, Nanney LB, et al. Transforming growth factor beta 1 (TGF-beta 1) induced neutrophil recruitment to synovial tissues: implications for TGF-beta-driven synovial inflammation and hyperplasia. *J Exp Med.* 1991;173(5):1121-32.
49. Reibman J, Meixler S, Lee TC, Gold LI, Cronstein BN, Haines KA, et al. Transforming growth factor beta 1, a potent chemoattractant for human neutrophils, bypasses classic signal-transduction pathways. *Proc Natl Acad Sci U S A.* 1991;88(15):6805-9.
50. Brandes ME, Mai UE, Ohura K, and Wahl SM. Type I transforming growth factor-beta receptors on neutrophils mediate chemotaxis to transforming growth factor-beta. *J Immunol.* 1991;147(5):1600-6.
51. Kim JS, Kim JG, Moon MY, Jeon CY, Won HY, Kim HJ, et al. Transforming growth factor-beta1 regulates macrophage migration via RhoA. *Blood.* 2006;108(6):1821-9.
52. Olieslagers S, Pardali E, Tchaikovski V, ten Dijke P, and Waltenberger J. TGF-β1/ALK5-induced monocyte migration involves PI3K and p38 pathways and is not negatively affected by diabetes mellitus. *Cardiovasc Res.* 2011;91(3):510-8.
53. Lodyga M, and Hinz B. TGF-β1 - A truly transforming growth factor in fibrosis and immunity. *Semin Cell Dev Biol.* 2020;101:123-39.
54. Stepien DM, Hwang C, Marini S, Pagani CA, Sorkin M, Visser ND, et al. Tuning Macrophage Phenotype to Mitigate Skeletal Muscle Fibrosis. *J Immunol.* 2020;204(8):2203-15.
55. Kiritsi D, and Nyström A. The role of TGFβ in wound healing pathologies. *Mech Ageing Dev.* 2018;172:51-8.
56. Davis MD, Suzaki I, Kawano S, Komiya K, Cai Q, Oh Y, et al. Tissue Factor Facilitates Wound Healing in Human Airway Epithelial Cells. *Chest.* 2019;155(3):534-9.
57. Frangogiannis NG. Transforming growth factor–β in tissue fibrosis. *Journal of Experimental Medicine.* 2020;217(3).
58. Desmoulière A, Geinoz A, Gabbiani F, and Gabbiani G. Transforming growth factor-beta 1 induces alpha-smooth muscle actin expression in granulation tissue myofibroblasts and in quiescent and growing cultured fibroblasts. *J Cell Biol.* 1993;122(1):103-11.
59. Chang MK, Raggatt LJ, Alexander KA, Kuliwaba JS, Fazzalari NL, Schroder K, et al. Osteal tissue macrophages are intercalated throughout human and mouse bone lining tissues and regulate osteoblast function in vitro and in vivo. *J Immunol.* 2008;181(2):1232-44.
60. Wang W, Chun H, Baek J, Sadik JE, Shirazyan A, Razavi P, et al. The TGFbeta type I receptor TGFbetaRI functions as an inhibitor of BMP signaling in cartilage. *Proc Natl Acad Sci U S A.* 2019;116(31):15570-9.
61. de Kroon LM, Narcisi R, Blaney Davidson EN, Cleary MA, van Beuningen HM, Koevoet WJ, et al. Activin Receptor-Like Kinase Receptors ALK5 and ALK1 Are Both Required for TGFbeta-Induced Chondrogenic Differentiation of Human Bone Marrow-Derived Mesenchymal Stem Cells. *PLoS One.* 2015;10(12):e0146124.

62. Pittenger MF, Mackay AM, Beck SC, Jaiswal RK, Douglas R, Mosca JD, et al. Multilineage potential of adult human mesenchymal stem cells. *Science.* 1999;284(5411):143-7.
63. Wang W, Rigueur D, and Lyons KM. TGFβ signaling in cartilage development and maintenance. *Birth Defects Res C Embryo Today.* 2014;102(1):37-51.
64. Diederichs S, Baral K, Tanner M, and Richter W. Interplay between local versus soluble transforming growth factor-beta and fibrin scaffolds: role of cells and impact on human mesenchymal stem cell chondrogenesis. *Tissue Eng Part A.* 2012;18(11-12):1140-50.
65. Campbell MG, Cormier A, Ito S, Seed RI, Bondesson AJ, Lou J, et al. Cryo-EM Reveals Integrin-Mediated TGF-beta Activation without Release from Latent TGF-beta. *Cell.* 2020;180(3):490-501 e16.
66. Xu T, Wu M, Feng J, Lin X, and Gu Z. RhoA/Rho kinase signaling regulates transforming growth factor-beta1-induced chondrogenesis and actin organization of synovium-derived mesenchymal stem cells through interaction with the Smad pathway. *Int J Mol Med.* 2012;30(5):1119-25.
67. Foyt DA, Taheem DK, Ferreira SA, Norman MDA, Petzold J, Jell G, et al. Hypoxia impacts human MSC response to substrate stiffness during chondrogenic differentiation. *Acta Biomater.* 2019;89:73-83.
68. Chen PY, Qin L, Li G, Wang Z, Dahlman JE, Malagon-Lopez J, et al. Endothelial TGF-β signalling drives vascular inflammation and atherosclerosis. *Nat Metab.* 2019;1(9):912-26.
69. Cai L, Wang Z, Luo X, She W, and Zhang H. Optimal strategies for the prevention of heterotopic ossification after total hip arthroplasty: A network meta-analysis. *Int J Surg.* 2019;62:74-85.
70. Veltman ES, Lindenhovius AL, and Kloen P. Improvements in elbow motion after resection of heterotopic bone: a systematic review. *Strategies Trauma Limb Reconstr.* 2014;9(2):65-71.
71. Ripamonti U, Duneas N, Van Den Heever B, Bosch C, and Crooks J. Recombinant transforming growth factor-beta1 induces endochondral bone in the baboon and synergizes with recombinant osteogenic protein-1 (bone morphogenetic protein-7) to initiate rapid bone formation. *J Bone Miner Res.* 1997;12(10):1584-95.
72. Karasawa K, Asano K, Moriyama S, Ushiki M, Monya M, Iida M, et al. Vascular-resident CD169-positive monocytes and macrophages control neutrophil accumulation in the kidney with ischemia-reperfusion injury. *J Am Soc Nephrol.* 2015;26(4):896-906.
73. Asano K, Takahashi N, Ushiki M, Monya M, Aihara F, Kuboki E, et al. Intestinal CD169(+) macrophages initiate mucosal inflammation by secreting CCL8 that recruits inflammatory monocytes. *Nat Commun.* 2015;6:7802.
74. Ramirez F, Ryan DP, Gruning B, Bhardwaj V, Kilpert F, Richter AS, et al. deepTools2: a next generation web server for deep-sequencing data analysis. *Nucleic Acids Res.* 2016;44(W1):W160-5.
75. Robinson JT, Thorvaldsdottir H, Winckler W, Guttman M, Lander ES, Getz G, et al. Integrative genomics viewer. *Nat Biotechnol.* 2011;29(1):24-6.
76. Thorvaldsdottir H, Robinson JT, and Mesirov JP. Integrative Genomics Viewer (IGV): high-performance genomics data visualization and exploration. *Brief Bioinform.* 2013;14(2):178-92.

77. Martin-Malpartida P, Batet M, Kaczmarska Z, Freier R, Gomes T, Aragón E, et al. Structural basis for genome wide recognition of 5-bp GC motifs by SMAD transcription factors. *Nat Commun.* 2017;8(1):2070.
78. Agarwal S, Loder S, Brownley C, Cholok D, Mangiavini L, Li J, et al. Inhibition of Hif1alpha prevents both trauma-induced and genetic heterotopic ossification. *Proc Natl Acad Sci U S A.* 2016;113(3):E338-47.
79. Schindelin J, Arganda-Carreras I, Frise E, Kaynig V, Longair M, Pietzsch T, et al. Fiji: an open-source platform for biological-image analysis. *Nat Methods.* 2012;9(7):676-82.
80. Peterson JR, Okagbare PI, De La Rosa S, Cilwa KE, Perosky JE, Eboda ON, et al. Early detection of burn induced heterotopic ossification using transcutaneous Raman spectroscopy. *Bone.* 2013;54(1):28-34.
81. National Research Council Committee for the Update of the Guide for the C, and Use of Laboratory A. In: th ed. *Guide for the Care and Use of Laboratory Animals*. Washington (DC): National Academies Press (US), National Academy of Sciences.; 2011.

Figures and Figure Legends:

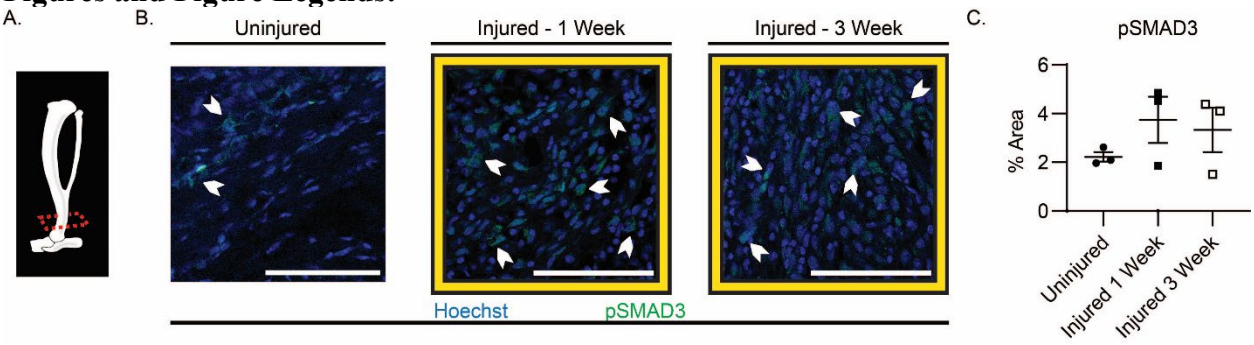

Figure 1. Canonical TGFβ signaling in the mouse distal hindlimb where HO forms. IF images, with **(A)** microCT graphic showing the histology section level used at timepoints indicated. **(B)** Effects of TGFβ signaling by proxy of pSMAD3 (green) and nuclear Hoechst (blue) in uninjured, 1 week post injury, and 3 weeks post injury. White chevrons to point out cells as examples of positive pSMAD3 staining. Scale bars represent 100 μm. **(C)** Quantification for % area of pSMAD3 at uninjured (n=3/group, 2-3 images/n) 1 week (n=3/group, 3 images/n), 3 weeks post injury (n=3/group, 3 images/n). Error bars represent mean ± SEM.

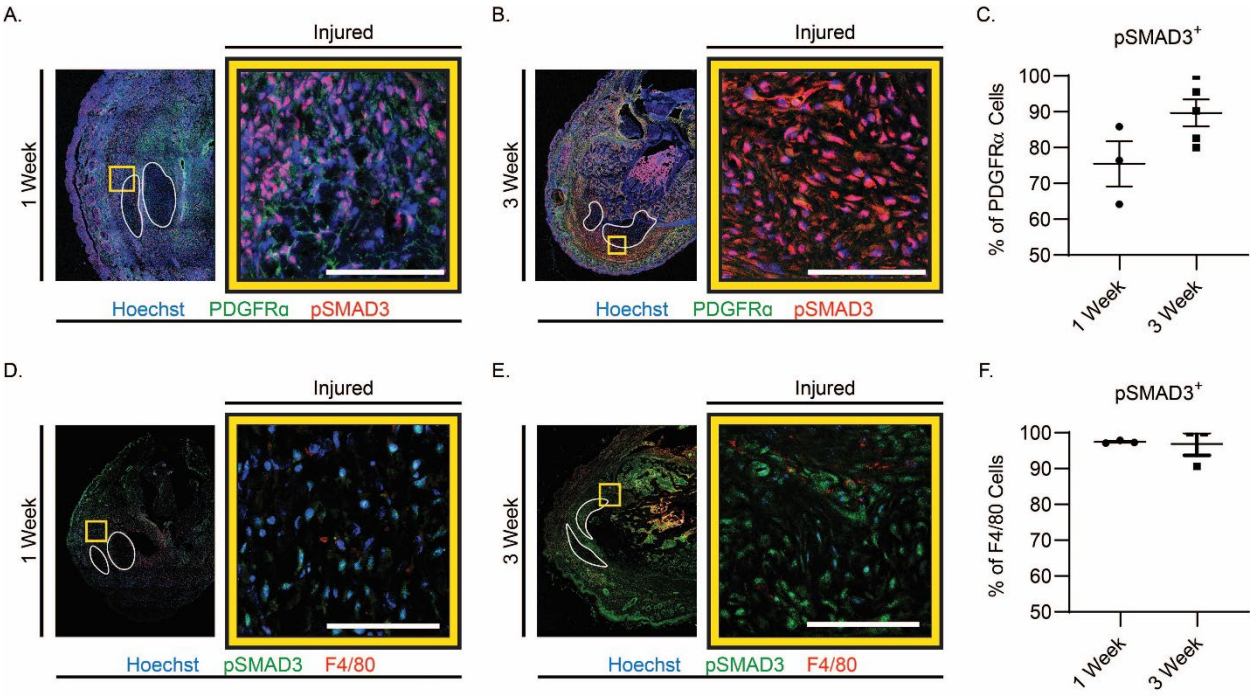

Figure 2. Canonical TGFβ signaling in MPC and macrophages. IF images, merged tile-scan with the tendons outlined in white and the yellow box showing the 63x zoomed in image to the right. Scale bars represent 100 μm and for quantifications, error bars represent mean ± SEM or median ± quartile. **(A)** IF images for pSMAD3 (red) in PDGFRα cells (green) and nuclear Hoechst (blue) for 1 week and **(B)** 3 weeks n=3 and 5/group), with **(C)** quantifications. **(D)** IF images are of pSMAD3 (green) in F4/80 cells (red) and nuclear Hoechst (blue) with quantifications for 1 week and **(E)** 3 weeks (n=3/group), with **(F)** quantification.

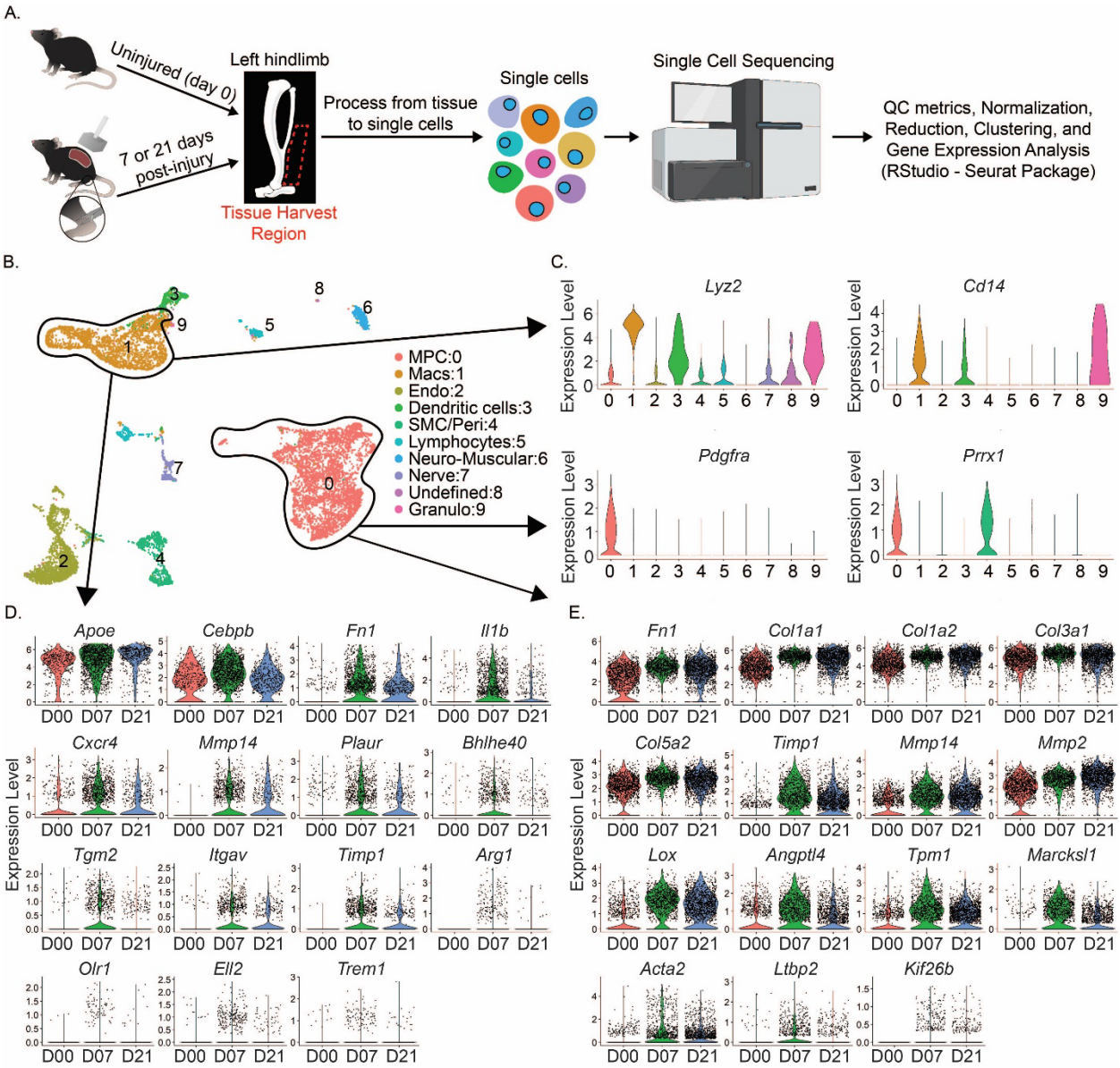

Figure 3. Single cell sequencing showing change in genes regulated by TGFβ signaling. (A) Overview of tissue to obtain results from scRNA-seq. **(B)** UMAP plot with all timepoints clustered and legend to the right of the plot. The MPC and Mac cluster are circled. **(C)** Violin plots of genes marking MPCs and Macs. **(D)** Genes regulated by TGFβ in Macs from day 0 (uninjured), day 7 and day 21. **(E)** Genes regulated by TGFβ in MPCs from day 0 (uninjured), day 7 and day 21.

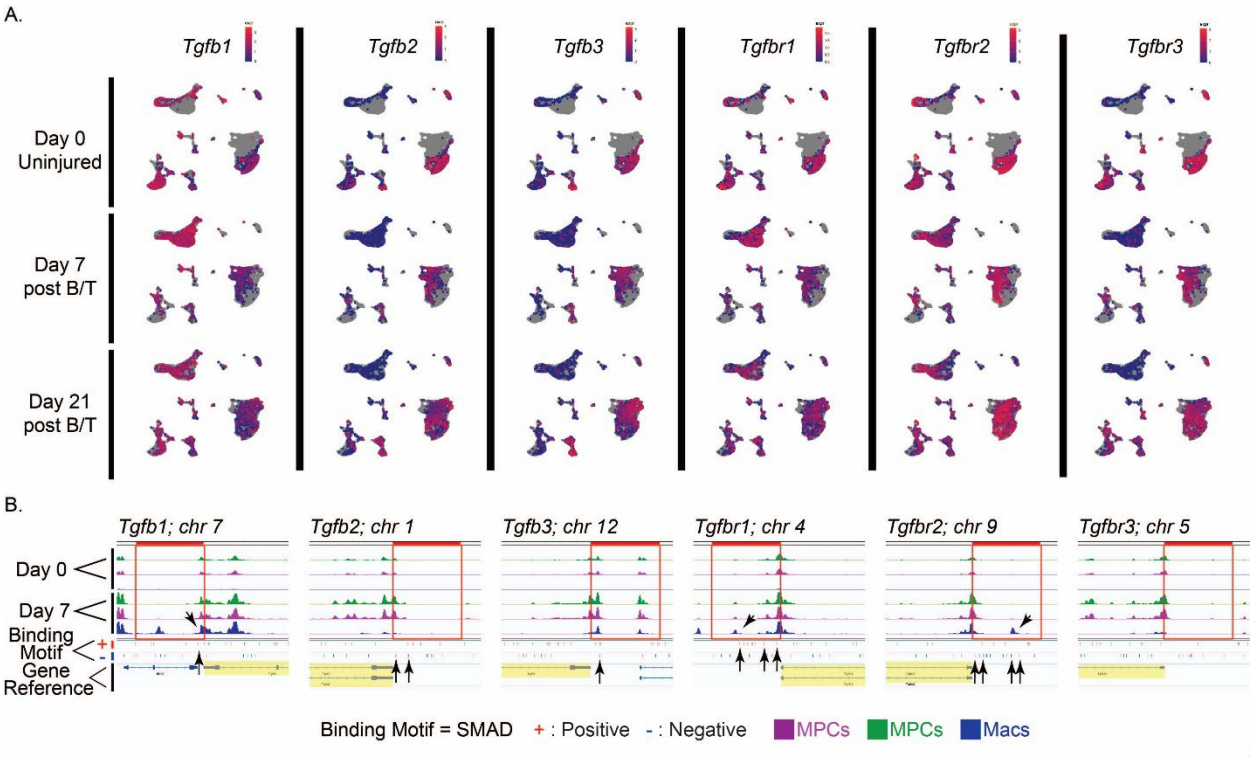

Figure 4. TGFβ downstream signaling in MPCs and macrophages with change in open chromatin for TGFβ ligands and receptors. (A) UMAP plots of TGFβ ligand and receptor genes for days 0, 7, and 21. **(B)** Images of open chromatin in promoter region by scATAC-seq associated with SMAD binding regions for TGFβ ligand and receptor genes stimulated by TGFβ. Highlighted yellow with a red box indicating ~5kb upstream promoter region. The tracks shown are color coded by their cluster identity such that green and magenta are MPCs and blue are Macs. All track data is presented in the range of 0 to 800. Black arrows are used to assist in indicating the regions of open chromatin at or near SMAD binding sites.

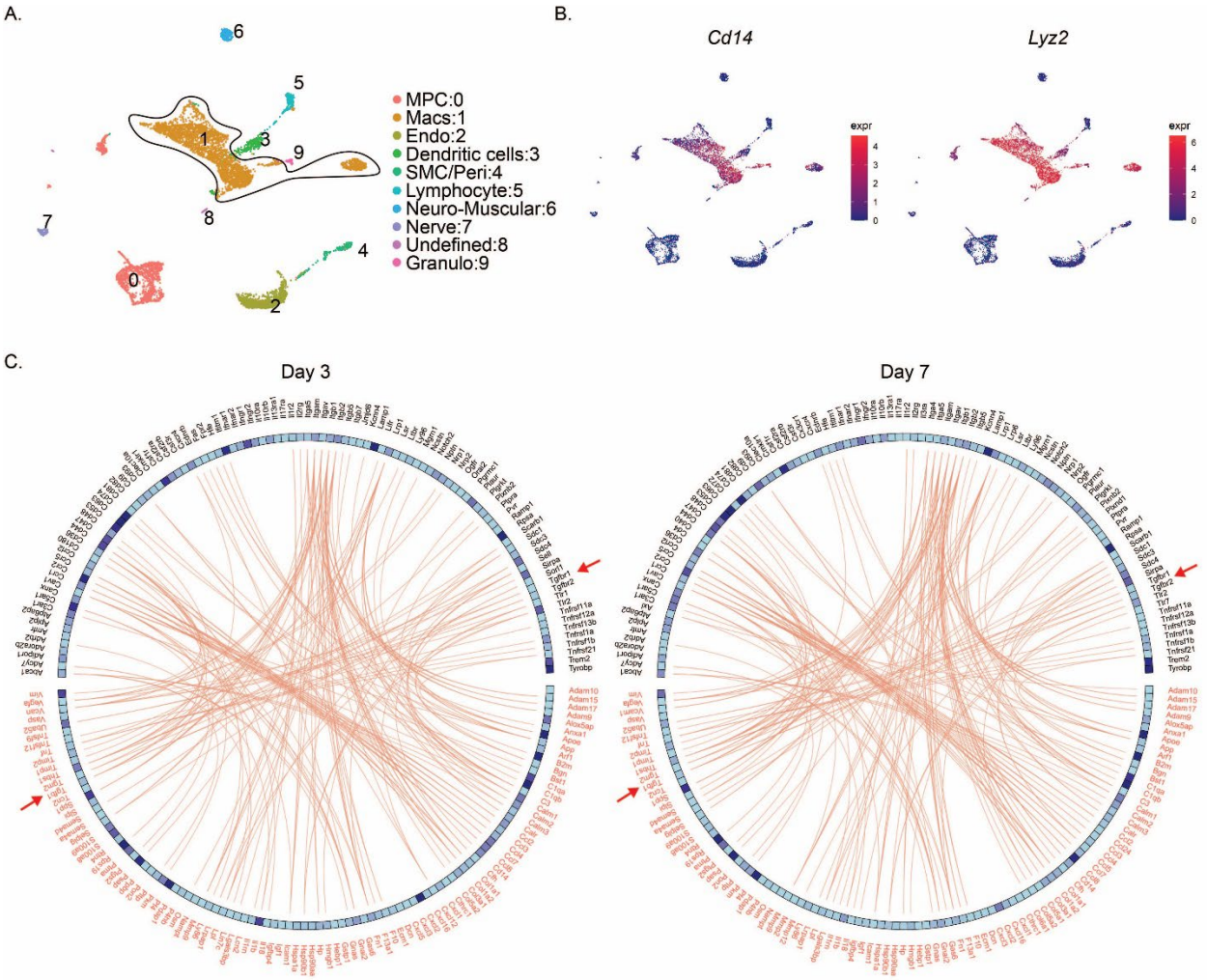

Figure 5. Ligand receptor signaling in macrophages. (A) UMAP plot of cells from day 0 and day 3 clustered with legend to the right of the plot. The composite Mac clusters are circled. **(B)** UMAP plots of genes marking Macs. **(C)** A list of ligand-receptor pairs was obtained from literature. The panel shows the top 100 expressed ligands-receptor pairs (red-black respectively), extracted from the Mac clusters at day 3 and day 7. Red arrows point to TGFβ1 signaling.

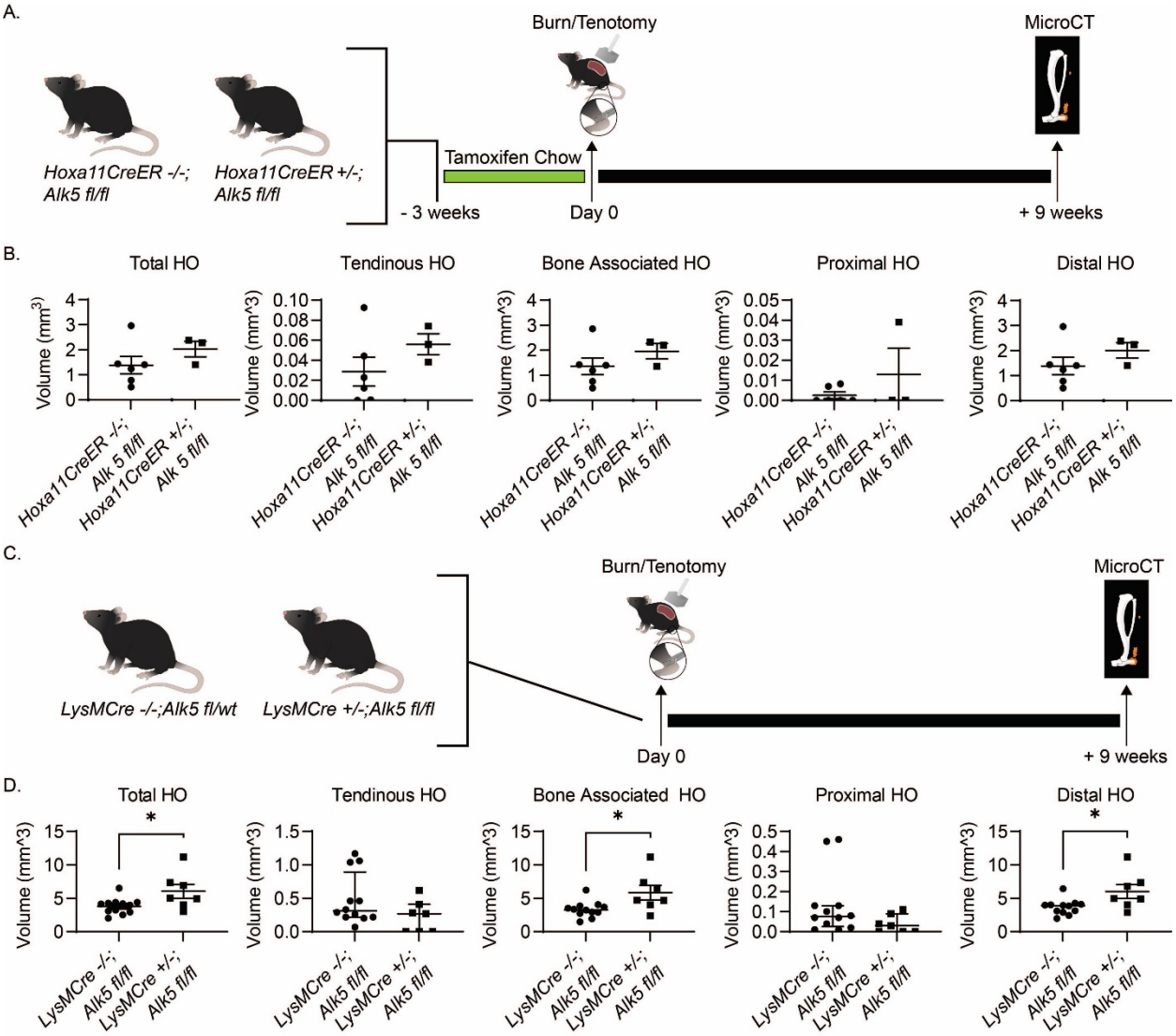

Figure 6. Loss of Alk5 signaling in macrophages but not in MPCs has a greater impact on trauma induced HO. (A) Graphic to depicting experimental timeline for *Hoxa11CreER^{T2}* mice. **(B)** MicroCT analysis of left injured hindlimb 9 weeks post injury for *Hoxa11CreER^{T2} -/-;Alk5fl/fl* compared to *Hoxa11CreER^{T2} +/-;Alk5fl/fl* (n=11 and 7 respectively/group) **(C)** Graphic to depicting experimental timeline for *LysMCre* mice. **(D)** MicroCT analysis of left injured hindlimb 9 weeks post injury for *LysMCre-/-;Alk5fl/fl*, *LysMCre+/-;Alk5fl/fl*. (n=12, 7 respectively/group). Error bars represent mean ± SEM or median ± interquartile range.

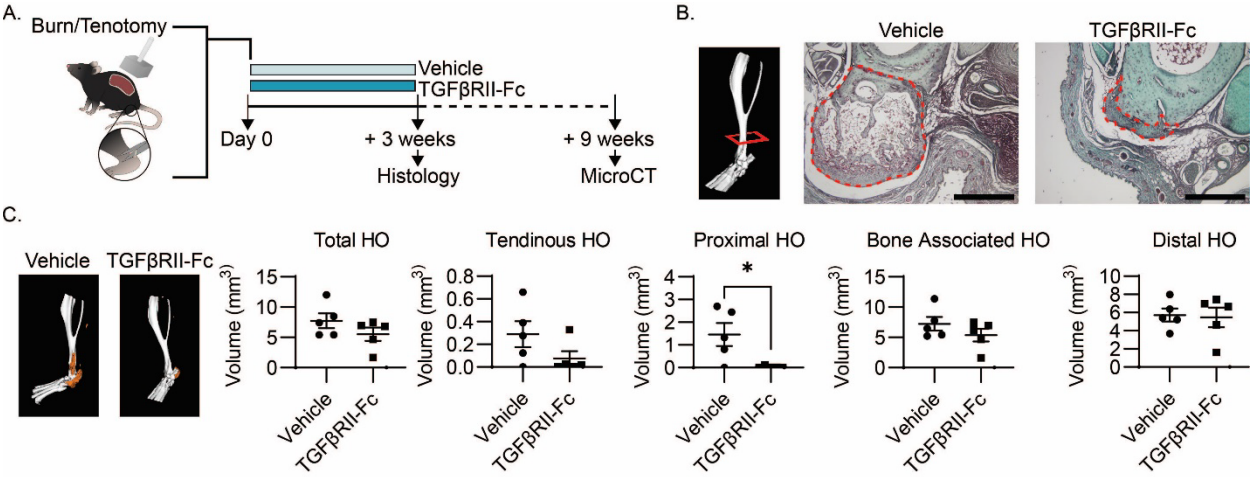

Figure 7. Effects of ligand trap (TGFβRII-Fc) treatment on HO formation. (A) Graphic to depict model and experiment. To the right is graphic depicting HO formation by microCT and the regions assessed and what those include. **(B)** Example microCT image with red box indicating the approximate level histologic sections were taken from. Safranin O stains of vehicle and ligand trap treated hindlimbs (n= 2/group). Region of HO is outlined in red. Scale bars represent 500 µm. **(C)** Top left: MicroCT reconstructions of representative samples where the HO is indicated in orange. To the right of and a row below are graphs of HO volume quantification with proximal HO showing significance by students t-test (n=5/group). Error bars represent mean ± SEM for parametric data.

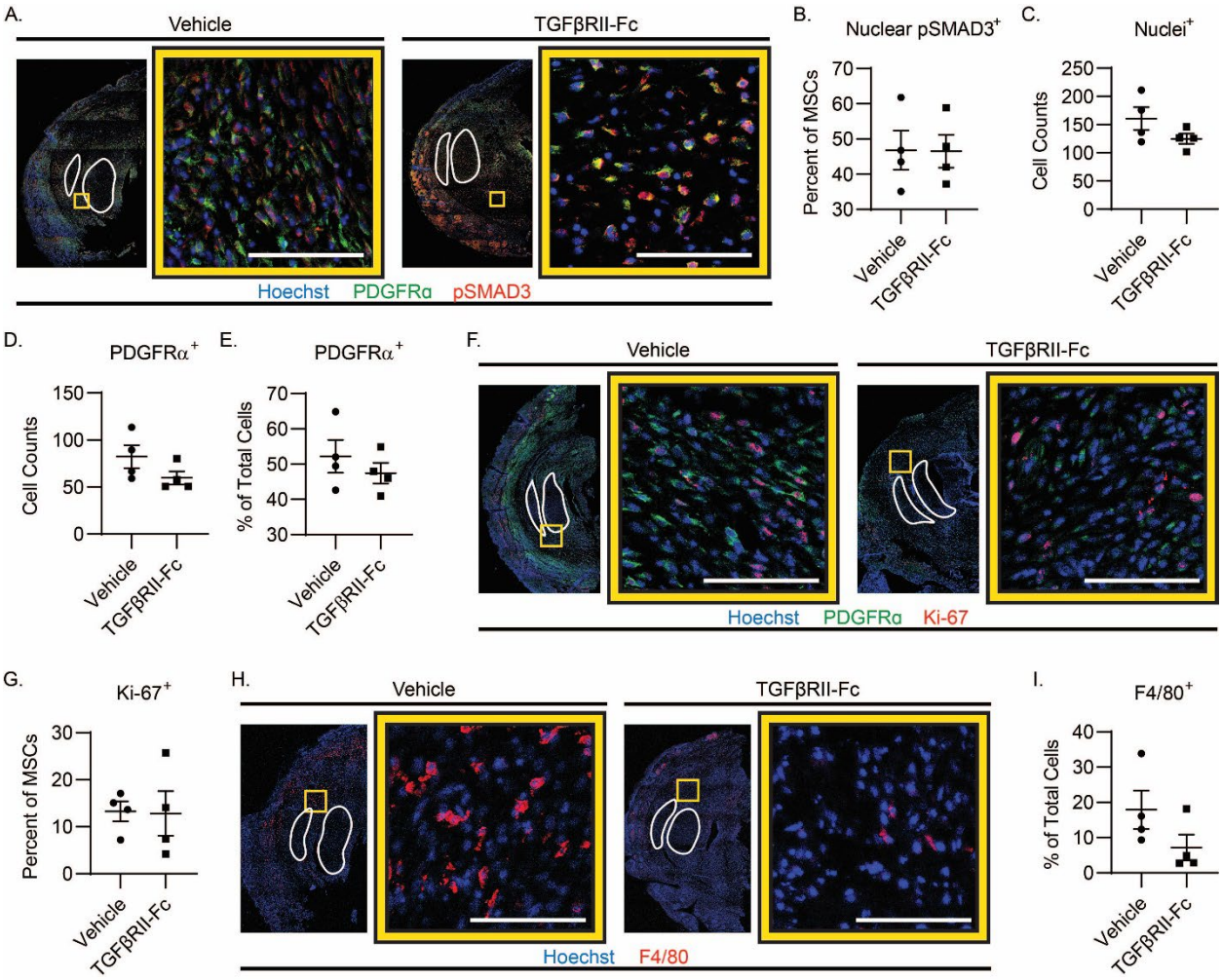

Figure 8. Ligand trap does not change in MSC canonical signaling or proliferation, but trend toward decreased macrophages. (A) Immunofluorescent tile-scans of the distal hindlimb where the tendons are outlined in white. The yellow box indicates the zoomed in image location to the right of the tile scan where the two groups are identified above the images and the color legend is below. **(B) C**anonical TGFβ signaling by pSMAD3 nuclear percent in PDGFRα+ (MPCs) cells (n=4/group, 3 images/n). **(C-E)** Further quantification from panel A, of the nuclei at injury site, total MPCs, and percent of MPCs from total. **(F)** IF images and **(G)** quantification of proliferation by anti-Ki-67 in MPCs (n=4/group, 3 images/n). **(H)** IF images and **(I)** quantification of percent of macrophages by anti-F4/80 (n=4/group, 2-3 images/n). Error bars presented in graphs represent mean ± SEM for parametric data and represent median ± quartile for non-parametric data. Scale bars represents 100 μm.

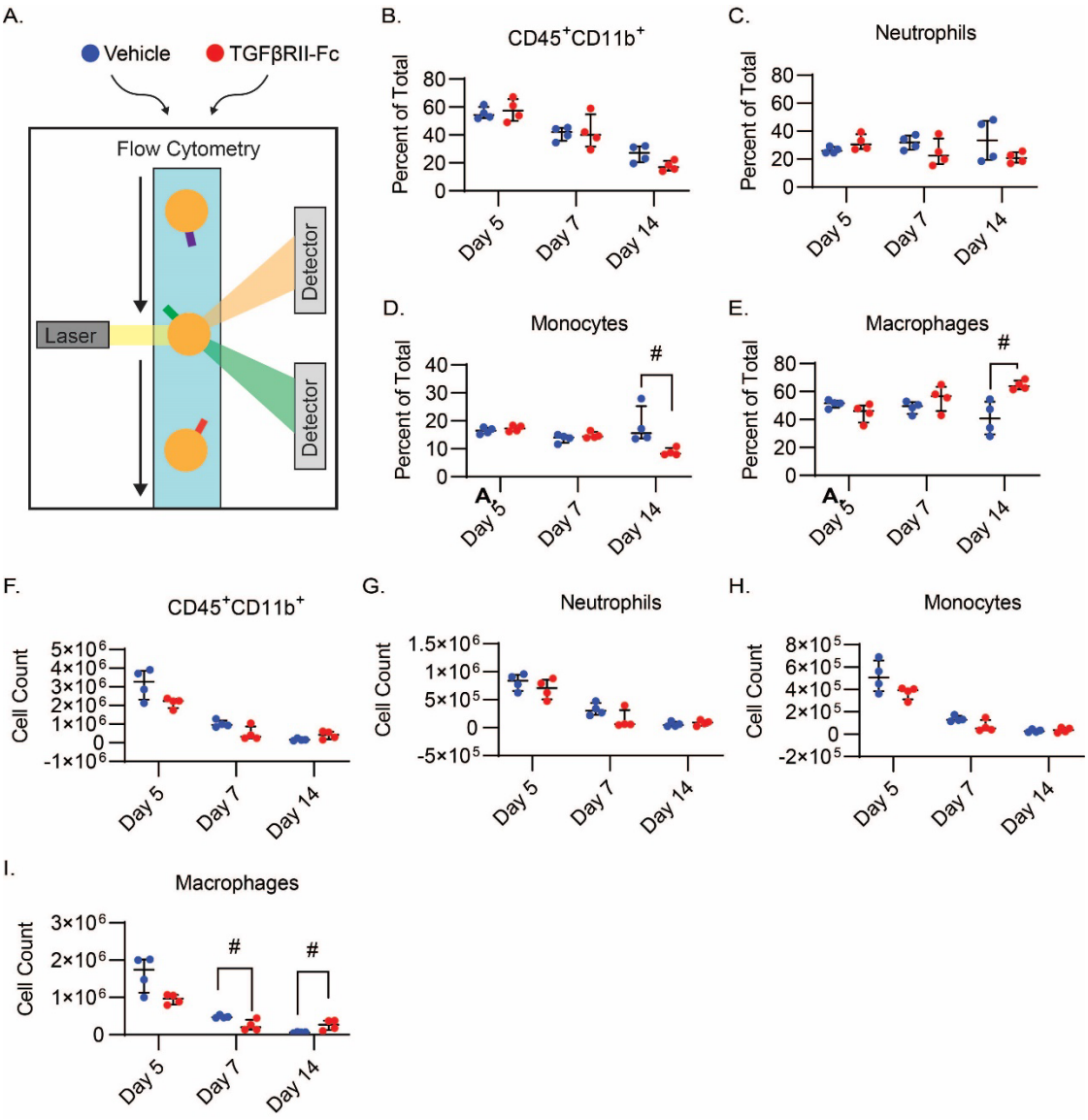

Figure 9. Flow cytometry shows treatment alters monocyte/macrophages at damaged left hind limb tissue. (A) Cell group legend each of which undergoes flow cytometry as depicted with a graphic and to the right are the results (3 time points, n=4/group). **(B-E)** Show the percent of total cells for CD45+CD11b+, Neutrophils, Monocytes and Macrophages. **(F-I)** shows the total cell counts. Error bars presented in graphs represent median ± quartile for non-parametric data.

Tables:

Table 1. Ligand binding parameters and inhibitory activity of TGFβRII-Fc.

	SPR			Cell-based assay
Ligand	k_a ($M^{-1}s^{-1}$)	k_d (s^{-1})	K_D (pM)	IC_{50} (pM)
TGFβ1	1.38×10^8	2.04×10^{-3}	14.8	22.9
TGFβ2	Transient binding		11,600	> 88,730
TGFβ3	1.16×10^8	1.30×10^{-3}	11.2	4.46

Table 2. Antibodies used in this study.

Antibody	Supplier	Catalog Number	IF Dilution	Flow Dilution
Anti-pSMAD3	Novus Biologicals	NBP1-77836	1:50	
Anti-F4/80	Abcam	ab6640	1:50	
Anti-Ly6G	Abcam	ab25377	1:50	
Anti-Ki67	Abcam	ab15580	1:50	
Anti-PDGFRa	R&D systems	AF1062	1:25	
Anti-TGFβR1	Sigma	ABF17-I	1:50	
Donkey anti-rabbit 488	Invitrogen	A21206	1:200	
Donkey anti-goat 488	Invitrogen	A11055	1:200	
Donkey anti-goat 594	Invitrogen	A11058	1:200	
Donkey anti-rabbit 594	Invitrogen	A21207	1:200	
Donkey anti-rat 594	Jackson	712-586-153	1:200	
Donkey anti-rat 488	Invitrogen	A21208	1:200	
Donkey anti-rabbit 647	Invitrogen	A31573	1:200	
Hoechst 33342	Invitrogen	H3570	1:2000	
Anti-mouse CD16/32	BD Pharmingen	553142		1:5
Anti-Ly6G-FITC		clone 1A8		1:200
Anti-CD11b-PeCy7		clone M1/70		1:1000
Anti-Ly6C-PerCP Cy5.5		clone HK1.4		1:200
Anti-CD45-PE		clone 30-F11		1:100